A 3D bioprinted hydrogel gut-on-chip with integrated electrodes for transepithelial electrical resistance (TEER) measurements

Biofabrication

PAPER

A 3D bioprinted hydrogel gut-on-chip with integrated electrodes for transepithelial electrical resistance (TEER) measurements

Daniel Vera[1], **María García-Díaz**[2], **Núria Torras**[2], **Óscar Castillo**[2], **Xavi Illa**[1,3], **Rosa Villa**[1,3], **Mar Alvarez**[1,3,*] and **Elena Martinez**[2,3,4,*]

[1] Instituto de Microelectrónica de Barcelona, IMB-CNM (CSIC), Bellaterra, Barcelona 08193, Spain
[2] Biomimetic Systems for Cell Engineering, Institute for Bioengineering of Catalonia (IBEC), The Barcelona Institute of Science and Technology, Barcelona 08028, Spain
[3] Centro de Investigación Biomédica en Red de Bioingeniería, Biomateriales y Nanomedicina, Instituto de Salud Carlos III, Barcelona 08193, Spain
[4] Department of Electronics and Biomedical Engineering, University of Barcelona (UB), Barcelona 08028, Spain
[*] Authors to whom any correspondence should be addressed.

E-mail: mar.alvarez@imb-cnm.csic.es and emartinez@ibecbarcelona.eu

Keywords: bioprinted, hydrogels, gut-on-a-chip, impedance spectroscopy, integrated electrodes, intestinal barrier, intestinal mucosa

Supplementary material for this article is available online

OPEN ACCESS

RECEIVED
20 September 2023

REVISED
29 January 2024

ACCEPTED FOR PUBLICATION
4 April 2024

PUBLISHED
12 April 2024

Abstract

Conventional gut-on-chip (GOC) models typically represent the epithelial layer of the gut tissue, neglecting other important components such as the stromal compartment and the extracellular matrix (ECM) that play crucial roles in maintaining intestinal barrier integrity and function. These models often employ hard, flat porous membranes for cell culture, thus failing to recapitulate the soft environment and complex 3D architecture of the intestinal mucosa. Alternatively, hydrogels have been recently introduced in GOCs as ECM analogs to support the co-culture of intestinal cells in *in vivo*-like configurations, and thus opening new opportunities in the organ-on-chip field. In this work, we present an innovative GOC device that includes a 3D bioprinted hydrogel channel replicating the intestinal villi architecture containing both the epithelial and stromal compartments of the gut mucosa. The bioprinted hydrogels successfully support both the encapsulation of fibroblasts and their co-culture with intestinal epithelial cells under physiological flow conditions. Moreover, we successfully integrated electrodes into the microfluidic system to monitor the barrier formation in real time via transepithelial electrical resistance measurements.

1. Introduction

The intestinal barrier is a key regulator of the homeostasis in the human body, acting both as a nutrient absorption site and a protective defense against pathogens [1, 2]. To better understand its physiopathology, there is a need to develop *in vitro* models that can recapitulate gut architectural complexity and multicellular population. Also, these models are needed to assist drug development processes. Conventional models of gut tissue mostly consist in culturing intestinal epithelial cells on top of porous plastic membranes to form tight monolayers under static culture conditions with no fluid flow [3, 4]. Therefore, despite being a useful approach that can be easily implemented, these static cell culture models are oversimplified, sometimes resulting in poor predictive outcomes [5].

To overcome some of these limitations, gut-on-chip (GOC) models have been established to replicate the dynamic conditions of intestinal peristaltic flow [6, 7]. In these advanced *in vitro* systems, intestinal cells are cultured within a microfluidic platform under perfusion, recreating key mechanical forces such as shear stress, to which epithelial barriers are exposed to in physiological conditions. However, most of the currently proposed GOC devices only represent the intestinal epithelium, neglecting the importance of the different compartments present in the intestinal mucosa. This tissue is composed of an epithelial cell monolayer lining the lumen and the lamina propria, a connective tissue layer located below the epithelium. The epithelium organizes itself in a three-dimensional (3D) manner with finger-like protrusions called villi and tissue invaginations called crypts, where spatially controlled cell proliferation

and differentiation occurs [8]. The lamina propria contains various types of cells such as fibroblasts, myofibroblasts and immune cells, along with blood vessels embedded in an extracellular matrix (ECM) [9]. As these systems are based on stiff and flat semi porous membranes, they cannot recapitulate neither the interactions between cells and the ECM nor the compartmentalized 3D structure of the tissue barrier found *in vivo*, thus reducing their physiological relevance as *in vitro* models [10–12]. To better represent the characteristics of the intestinal mucosa, hydrogels have been selected as suitable ECM-like substrates for intestinal *in vitro* models [13]. These materials are 3D networks of polymeric chains that can absorb high contents of fluids. Natural, synthetic or hybrid, they are biocompatible and mechanically tunable, having the ability to mimic the softness of the target tissue [14, 15]. Stromal cells can be encapsulated within their porous structure, while supporting the formation of an epithelial monolayer on top to include all the relevant components of the barrier in the model [16].

Considering their benefits, hydrogels have been proposed as an alternative to stiff polymeric membranes in organ-on-chip applications, as they can mimic the spatial *in vivo* architecture of tissue barriers under dynamic conditions [17]. In the case of GOC, natural hydrogels such as collagen and Matrigel have been employed to support intestinal cell culture in different studies. For instance, perfusable intestinal tubules were generated on a collagen-filled channel within a microfluidic chip [18]. The pre polymer solution was loaded via capillary force and polymerized in the central channel of the device to later support the formation of an epithelial monolayer. Permeability assays could then be performed to assess the integrity of the enterocyte cell barrier. Other groups have reproduced the 3D morphology of the intestinal epithelium by adapting different microfabrication techniques to integrate these engineered hydrogels in microfluidic setups. As an example, soft lithography was used to pattern collagen I—based hydrogels with villi-like pillars [19]. The substrate was placed in a microfluidic device where cells could grow and differentiate along the vertical pillars under gravity-driven flow. Combining 3D topographical features with flow-induced shear stress forces promoted cell polarization and key cellular functions such as metabolic activity and permeability compared to static cell cultures. In another approach, a hydrogel channel was patterned with crypt-like shapes via laser-based photoablation to allow the self-organization and differentiation of organoid-derived intestinal cells into tubular epithelia [20]. Epithelial cells were co-cultured with different cell types embedded in the hydrogel channel and present in the intestinal lamina propria, such as immune cells and mouse intestinal myofibroblasts. The stromal cells migrated within the scaffold and interacted with the epithelial cells under flow, demonstrating the ability of the intestinal model to establish an *in vivo*-like compartmentalized organization. However, while current hydrogel GOC models have successfully replicated key aspects of the intestinal mucosa, the proposed microfabrication techniques have several drawbacks as they rely either on cumbersome procedures or expensive equipment, limiting their potential applications in the field. Thus, new technologies that comprise both easy and affordable microfabrication techniques are required to develop the next hydrogel GOCs.

In addition, cell barrier characterization in these microfluidic devices mostly relies on permeability and immunostaining assays, which cannot provide fast readouts about the state of the tissue monolayer during its formation. To solve these limitations, several groups have successfully integrated electrodes within organ-on-chips to perform transepithelial electrical resistance (TEER) measurements, a non-invasive technique that correlates the electrical properties of the tissue barrier with their integrity and tightness [21]. By placing them close to the cell culture area, fast and accurate readouts of the electrical impedance of the cell monolayers can be obtained in real time to monitor their development and function under dynamic conditions [22, 23]. However, this approach has only been implemented for membrane-based microfluidic chips and, to this day, no 3D hydrogel organ-on-chips have been developed to integrate electrodes for real time TEER quantification.

Here, we present a GOC model based on a perfusable hydrogel channel with lateral villi-like shapes that reproduces the 3D spatial organization of the intestinal mucosa, including the epithelial and stromal compartments. A high resolution digital light projection stereolithographic (DLP-SLA) bioprinting technique was used to generate the biomimetic hydrogels in a rapid and precise manner [24], while allowing their integration into a tri channel microfluidic chip. Based on previous studies, a hybrid pre polymer solution of poly(ethylene glycol) diacrylate (PEGDA) and gelatine methacryloyl (GelMA) was selected as a photosensitive bioink to fabricate the scaffolds [16, 24]. We demonstrated the ability to generate the biomimetic hydrogel channels by finely tuning the main printing parameters. To represent the stromal–epithelial interactions in the *in vitro* model, fibroblasts were embedded in the hydrogel, supporting the formation of an epithelial barrier on the channel for 2 weeks under continuous media perfusion. Immunostaining of the samples revealed the expression of tight junction markers associated to the epithelia while apparent permeability values suggested

the presence of a formed barrier. Also, the presented technology allowed the integration of electrodes within a hydrogel organ-on-chip system for the first time to study quantitatively the integrity of the intestinal cell barrier. This configuration enabled a real time recording of the TEER of the intestinal barrier via electrical impedance spectroscopy (EIS). With this device, values close to the physiological range could be recorded during dynamic cell culture. This system can thus provide a highly reliable strategy to assess in real time the function of epithelial barriers under dynamic conditions in complex *in vitro* models of the intestinal mucosa.

2. Materials and methods

2.1. 3D bioprinting of hydrogel channels

To fabricate the hydrogel channels, a customized DLP-SLA 3D printing setup based on a commercial SLA 3D printer (SOLUS; Junction3D) was used [24]. The system was adapted to print hydrogels with reduced sizes (less than 10 mm in diameter) using small volumes of pre polymer solution (less than 2 ml), while keeping the bioink at 37 °C using a built-in heater with a thermostat (TUTCO) that allows cell-laden hydrogel printing and prevents thermal gelation. A fluorinated ethylene propylene plastic film was attached to the bottom of the vat to create a gas permeable transparent window for the patterned light to reach the pre polymer solution. This created an oxygen gradient within the pre polymer solution, inhibiting the crosslinking reaction at the liquid–film interface, and preventing the hydrogel from sticking to the bottom of the vat. The light projector was used to project light from the bottom of the vat for patterned hydrogel polymerization. To prevent cell damage due to infrared (IR) radiation exposure, a short pass heat protection filter (KG3 SCHOTT, Edmund Optics) was attached to the 3D printer. The optical power density of the projector was set to 12.3 W cm^{-2} in the 320 nm to 640 nm wavelength spectral range.

To print the hydrogels, two main CAD designs of 3D hydrogel channels were created: one with two rectangular-shaped hydrogels with vertical flat walls separated by a central channel, and another design with two hydrogels with lateral pillars on the vertical walls facing the central channel to mimic the shape of the intestinal villi found *in vivo*. Different geometries were tested to obtain optimal encasing of the hydrogel within the chip while preserving the shape of the designed hydrogel channels. The tested printing parameters were defined as follows: layer thickness between 10 and 20 μm and normal layer exposure time between 1 and 10 s. The hydrogels were printed on a polyethylene terephthalate (PET) substrate (125 μm; Dupont Melinex ST504), attached to the bottom side of the printing support with a pressure sensitive adhesive (PSA) (ArCare® 92 712, Adhesive Research). The PET substrates were previously cut with a cutting plotter (Silhouette Cameo 4) to create 12 mm diameter circles, and then silanized with (trimethoxysilyl)propyl methacrylate (TSPMA; Sigma-Aldrich) for improved hydrogel attachment. The pre polymer solution was then loaded into the vat at 37 °C before the printing started. During the printing process, the hydrogel was photopolymerized in a layer-by-layer procedure by sequentially projecting white and black patterns generated from the z-sliced version of the 3D CAD design. Once the printing was completed, the substrate with the attached hydrogel was rinsed with warm PBS supplemented with 1% v/v penicilin/streptomycin (P/S), and gently dried with clean room wipes to remove unreacted bioink residues. Visual characterization of the hydrogels was performed with a stereomicroscope (Olympus, SZX2-ILLB) and images were analyzed with ImageJ software (http://imagej.nih.gov/ij, NIH).

2.2. Bioink composition

A GelMA-PEGDA pre polymer solution was prepared as a bioink to print the hydrogels. GelMA was synthesized using a previously described procedure [25]. The selected following composition was: 3% (w/v) PEGDA, with a molecular weight of 4000 Da (Sigma-Aldrich), 5% (w/v) GelMA, 0.4% (w/v) lithium phenyl-2,4,6-trimethylbenzoylphosphinate (LAP; TCI chemicals) photoinitiator and 0.025% (w/v) tartrazine (Sigma-Aldrich) food dye [24]. The components were added in a small vial wrapped in aluminum paper to avoid light exposure and dissolved in Hank's Balanced Salt Solution (Gibco, ThermoFisher Scientific) supplemented with 1% (v/v) P/S at 65 °C in a water bath under stirring conditions for 2 h. The dissolved solution was kept at 37 °C for at least 30 min before its use. For cell-laden hydrogel fabrication, cells were directly mixed with the warm pre polymer solution before printing.

2.3. Design and fabrication of the microfluidic chip

A multi-layer microfluidic device with three independent channels was designed to encase the printed hydrogel channel within a central chamber for dynamic cell culture. The device (width: 25 mm, length: 40 mm) consisted of two top and bottom plates and a middle piece containing the parallel channels. The plates were made of cyclic olefin polymer (COP, 2 mm, Zeonor; ChipShop) and fabricated with inlet holes and screw holes respectively using a computer numerically controlled milling machine (MDX-40A; Roland Digital) [26]. Male mini-luer connectors (ChipShop) were glued to the top plate inlet holes with a photocurable silicone adhesive (Loctite 3104, Henkel). The middle part (COP, 1 mm, Zeonor; ChipShop) was also milled to reduce the height of the substrate according to the thickness of the encased hydrogel (between 300 and 800 μm) and to define the channels and central chamber. To

enclose the channels at the top and bottom, patterned COP foils (125 μm, Topas; ChipShop) were cut with a cutting plotter (CAMM-1 Servo GX24, Roland DG Corporation) and bonded to the middle piece with double-sided PSA (ArCare® 92 712, Adhesives Research). Two silicone sheets of 1 mm (platinum cured sheet, Silex) were also cut with the cutting plotter to be used as sealing gaskets.

After the printing, the circular PET substrate with the hydrogel channel was attached to the bottom of the middle piece to encase the scaffold in the central chamber of the chip, acting as a separator between the three channels. Finally, screws were used to assemble the device by clamping the middle piece containing the hydrogel between the top and bottom silicone sheets and COP plates to prevent leakage in the chip.

2.4. Microfluidic perfusion for cell culture on-chip

As a preliminary step, 3D finite element method (FEM) simulations of the central channel were performed to select suitable flow conditions in the hydrogel GOC. The range of fluid shear stress (FSS) exerted on the epithelial cells grown on the hydrogel was computed under different fluid flows and channel geometries, either with rectangular-shaped or lateral pillar-sided hydrogels. Using the COMSOL (COMSOL Multiphysics v5.6) CFD module, flow velocity profiles were modeled along the central channel, where epithelial cells are present. Shear stress was computed as the product of shear rate (unit: s^{-1}) and fluid viscosity (unit: Pa·s). Simulation parameters were defined according to the fluid properties and channel dimensions.

To support cell culture under dynamic conditions, the chip was connected to a closed loop microfluidic setup where each channel was perfused independently. A peristaltic pump (Reglo ICC; Ismatec, Cole Parmer) was used to generate a continuous flow within the microfluidic devices. Silicone extension tubing (inner diameter: 0.51 mm, Freudenberg Medical) was used to connect the pump system to the chips placed inside the incubator. Sterile passive bubble filters (Speedflow Kids; Gvs) were also added in-line at the chip inlets to reduce the risk of bubble formation. All components (tubing and adapters) of the microfluidic setup and the chip were sterilized via autoclaving followed by overnight drying.

2.5. Cell culture

Mouse NIH-3T3 cells (ATCC® CRL-1658™) were used in our model to represent the fibroblasts present in the stromal compartment of the intestinal mucosa. The cells were grown and maintained in 175 cm^2 flasks at 37 °C, 5% CO_2 using high-glucose DMEM media (Glutamax supplement, Gibco; ThermoFisher Scientific), supplemented with 10% (v/v) fetal bovine serum (FBS, Gibco; ThermoFisher Scientific) and 1% (v/v) P/S (Sigma-Aldrich). Fibroblasts were passaged twice a week and harvested for cell culture experiments.

Human colorectal adenocarcinoma Caco-2 cells (ATCC® HTB-37™) were used to reproduce the intestinal epithelium in our model. They were grown and maintained in 75 cm^2 flasks at 37 °C, 5% CO_2 in high-glucose DMEM media (Glutamax supplement, Gibco; ThermoFisher Scientific), supplemented with 10% (v/v) FBS (Gibco; ThermoFisher Scientific), 1% (v/v) non-essential amino acids (NEAA, Gibco; ThermoFisher Scientific), and 1% (v/v) P/S (Sigma-Aldrich), and harvested for cell culture experiments. Caco-2 cells were passaged every week and medium was refreshed every 2–3 d.

2.6. Fabrication of the bioprinted intestinal stromal compartment

To mimic the stromal compartment of the intestinal mucosa in the GOC model, NIH-3T3 fibroblasts were encapsulated in the bioprinted hydrogel channels. The cells cultured in flasks were trypsinized and resuspended in the GelMA-PEGDA pre polymer solution with a cell density of 7.5 × 10^6 cells ml^{-1}. After this, the cell-laden bioink was loaded into the vat at 37 °C and hydrogel channels were printed on silanized PET substrates using the following printing parameters: layer exposure time of 5 s and layer thickness of 13 μm. Once printed, samples were cleaned with PBS supplemented with 1% (v/v) P/S, gently dried with clean room wipes to remove unreacted residues and finally detached from the printing support to be placed into a sterile 24 well-plate with NIH-3T3 cell culture medium with 0.3% (v/v) Normocin (Invitrogen) inside the incubator before chip assembly. Cell-laden hydrogel channels were encased in the central chamber of the microfluidic chip by attaching the substrate to the bottom PSA layer of the middle piece. The chip was then assembled and shortly after, warm cell culture medium was manually loaded into the three channels to avoid cell death and hydrogel dehydration. Finally, the chip was connected to the microfluidic setup and all the components except the pump were placed inside the incubator at 37 °C. Recirculating medium was perfused continuously along the channels from two different reservoirs, one for the lateral channels and another one for the central channel, with a flow rate of 5 μl min^{-1} (for 500 μm thick hydrogels) to support cell culture of the hydrogel-embedded NIH-3T3 cells for 3 or 4 d.

The cell viability of hydrogel-embedded NIH-3T3 fibroblasts cultured on-chip was assessed with a Live/Dead™ cytotoxicity kit assay (Invitrogen) 1 and 4 d after cell encapsulation and perfusion. To perform the assay, the chip was disassembled, and the sample was carefully retrieved from the device. Calcein AM and ethidium homodimer-1 (EthD-1) were added to stain live and dead cells respectively. Hoescht was used to stain the nuclei. Afterwards,

the samples were analyzed via confocal laser-scanning microscopy (LSM800; Zeiss). The quantification of live and dead cells was done with a manual counter on ImageJ 1.53t software (NIH; open source).

2.7. Intestinal epithelial cell seeding

To represent the epithelial compartment in our 3D GOC model, Caco-2 cells were seeded on the cell-laden hydrogel channel with a cell density of 7.5×10^5 cells cm^{-2} (10^7 cells ml^{-1}) after 3 or 4 d of culturing hydrogel-embedded NIH-3T3 fibroblasts under flow. For the seeding procedure, the chips were disconnected from the microfluidic setup and Caco-2 cell culture medium with 0.3% (v/v) Normocin (Invitrogen) and the resuspended cells was loaded manually into the central channel. To allow the cells to sediment on the hydrogel walls, the chips were placed vertically on each side in the incubator for 2 h each time. Microfluidic perfusion was restarted afterwards with a flow rate of 10 μl min^{-1} (for a 500 μm thick hydrogel channel) in all channels for 14 d. Cells inside the chip were inspected under the brightfield optical microscope (ECLIPSE Ts2 Optical Microscope, Nikon) every 2 d to assess formation of an epithelial barrier, and medium from the reservoirs was replaced every 5–6 d.

2.8. Immunofluorescence staining

Cells were fixed and immunostained after 14 d of cell culture in the chips to assess the distribution of hydrogel-embedded NIH-3T3 fibroblasts and the presence of tight junction markers for epithelial Caco-2 cells. To preserve the integrity of the epithelial cell barrier on the hydrogel channel, the immunostaining assay was performed inside the chips. The chips were disconnected from the microfluidic setup and reconnected to a syringe pump (NE-1000 Programmable Single Syringe Pump, New Era) to perfuse the buffers with flow rates between 5 and 10 μl min^{-1}. Samples were fixed with 10% buffered formalin solution (Sigma-Aldrich) for 1 h at room temperature. Afterwards, samples were washed with PBS under flow and permeabilized with 0.5% (v/v) TritonX (Sigma-Aldrich) in static conditions for 2 h. Following this, a blocking solution containing 1% (w/v) bovine serum albumin (Sigma-Aldrich), 3% (v/v) donkey serum (Milipore) and 0.3% (v/v) TritonX (Sigma-Aldrich) was loaded in all channels and left for incubation under shaking conditions overnight at 4 °C. Once the blocking step was completed, primary antibodies against Zonula-Occludens-1 (2.5 μg ml^{-1}) (ZO-1, 40-2200, ThermoFisher Scientific), β-Catenin (1 μg ml^{-1}) (ab2365, Abcam) and collagen IV (134 001, Biorad) in working buffer solution were loaded into the channels and incubated at 4 °C under shaking conditions overnight. Finally, chips were washed with PBS for 3–4 h under continuous flow to remove unbounded primary antibodies and the secondary antibody working buffer containing donkey anti-mouse Alexa A488 (4 μg ml^{-1}) (Invitrogen, ThermoFisher Scientific), donkey anti-rabbit Alexa A647 (4 μg ml^{-1}) (Invitrogen, ThermoFisher Scientific), DAPI (5 μg ml^{-1}) (ThermoFisher Scientific) and Rhodamine-phalloidin (0.07 μM) (Cytoskeleton) was loaded into the chip and left for incubation 2 h under shaking conditions at 4 °C.

Immunostained samples were first imaged inside the chip with a fluorescence inverted microscope (Leica Thunder). Later, the chip was disassembled and the substrate with the hydrogels was carefully retrieved for confocal imaging (LSM 800; Zeiss) to obtain images at a higher magnification. The acquired images were treated on ImageJ 1.53t software (NIH; open source).

2.9. Electrical sensitivity analysis for electrode design

To evaluate the current density distribution across the central cell culture chamber with the integrated electrodes and identify potential TEER measurement errors, a 3D FEM study was performed on COMSOL Multiphysics 5.6 with the AC/DC module. A two-electrode configuration design with each electrode covering the top part of each lateral channel was considered. Each electrode worked either as a working or counter electrode and current flowed through the hydrogel channel, measuring the total TEER of cell barriers located on both walls of the central channel. A rectangular hydrogel channel (width: 1 mm; length: 7 mm; height: 0.5 mm) was considered for the computations, and the cell barrier was modeled as a contact impedance with a given conductivity on each lateral wall of the central channel. Different TEER values were attributed to the cell barrier in the simulations, ranging from 10° to 10^3 $\Omega \cdot cm^2$. The rest of the outer boundaries were defined as electrical insulators. The electrical sensitivity was calculated from the computed current densities across the hydrogel channel to determine which areas of the cell barrier contribute the most and the least for each TEER value [27]. The obtained values were normalized by the cell barrier area. When the normalized sensitivity was close to 1 and uniform over the cell barrier area, the electrode configuration would ensure a homogenous current density distribution and an accurate TEER measurement within the device.

2.10. Fabrication and characterization of the integrated electrodes

To integrate the electrodes in the microfluidic chip, a 180 mm diameter plastic COP foil (125 μm, Topas; ChipShop) was initially cut with a cutting plotter (CAMM-1 Servo GX-24; Roland) and used as a substrate. An adhesive vinyl shadow mask with the electrode patterns was also cut with the plotter and attached to the foil. Following this, a 20/200 nm

titanium/gold (Ti/Au) bilayer was deposited on the plastic substrate by e-beam evaporation [26]. The Ti layer was used to improve the bonding between gold and the plastic substrate. The COP foil was then cut in 40 × 25 mm rectangles matching the dimensions of the chip with all the inlets and outlet holes, and the shadow mask was then removed. A double-sided PSA (ArCare® 92 712, Adhesives Research) was used as a passivation layer for the electrodes. Electrical wires and pins were soldered to connect the chip to the external electrical equipment. Moreover, electrochemical platinization of the patterned gold electrodes was performed to reduce their polarization impedance [28]. Finally, a chloride solution containing hydrochloric acid 0.1 M, 2.3% platinum (Pt) (IV) chloride, and 0.023% lead (IV) 99% acetate was used to deposit platinum black on the active area of the electrodes with a custom setup connected to a potentiostat (Solartron SI 1287) by applying a potential of −0.2 V during 30 s (CorrWare software) to generate the electrochemical reaction.

The polarization impedance of the gold electrodes was characterized before and after Pt black deposition via EIS. For that, the pair was connected to an impedance analyzer (Solartron SI 1260) and an AC voltage signal of 10 mV was applied at selected frequencies in the range between 10° Hz and 10^6 Hz. The resulting impedance spectra were compared to evaluate the effect of the platinization on the properties of the electrodes. Once the electrodes were validated, the PSA liner of the passivation layer was removed, and the patterned chip substrate was bonded to the rest of the middle component of the chip.

2.11. Characterization of the intestinal barrier

2.11.1. EIS-based TEER monitoring

To quantify the integrity of the epithelial cell barrier, TEER measurements were performed in real time during cell culture on-chip inside the incubator. The integrated electrodes were connected to a commercial potentiostat (PalmSens 4) in a two-point configuration. An AC voltage excitation signal of 10 mV was applied to measure the total impedance. Impedance spectra were recorded in the frequency range between 10 Hz to 1 MHz via EIS in time intervals of 15 or 30 min.

2.11.2. Permeability assay

Permeability assays were performed inside the device after 14 d of microfluidic cell culture since epithelial cell seeding. The device was first placed under a fluorescence microscope (Leica Thunder) equipped with an incubator system at 37 °C, 5% CO_2. The chip was then connected to a pump and a fluorescent dextran with a molecular weight of 70 kDa (FD70, Sigma-Aldrich) was perfused through the central channel at a flow rate of 10 μl min^{-1} for 90 min. The lateral diffusion of the dye across the two adjacent hydrogels was recorded within the central area of the chip every 10 min. The recorded images of the hydrogel channel were then analyzed to extract the fluorescence intensity profiles at different areas of interest with Fiji software, and to calculate the apparent permeability of the cell barrier [18, 29]. To do this, the average fluorescence intensity of the considered hydrogel region was divided by the average fluorescence intensity of the selected region of the central channel. Assuming a proportional relationship between the dextran concentration and the fluorescence intensity, P_{app} could be determined:

$$P_{app} = \frac{\Delta I_{f,gel} * V_{gel}}{\Delta t * A_{barrier} * I_{f,channel}}$$

where $\Delta I_{f,gel}$ is the difference of average fluorescence intensity in the hydrogel channel between $t = 0$ and $t = 90$ min. V_{gel} is the volume of the hydrogel region where fluorescence is quantified. Δt is the time of the experiment. $A_{barrier}$ is the area of the hydrogel channel lateral edge. $I_{f,channel}$ is the average fluorescence intensity of the central channel where the dextran is perfused. The apparent permeability was calculated for cell-free hydrogels, defined as controls, and hydrogel channels with co-cultured 3T3 fibroblasts and Caco-2 cells to evaluate the diffusion of the dextran through the epithelial barrier.

2.12. Data representation and analysis

Plot values are displayed as the mean ± standard deviation (SD). OriginPro 9.60 (OriginLab) was used to generate the graphs. Student's paired *t*-tests were run to compare groups of data to determine their difference. $p < 0.05$ was used as a threshold to confirm the statistical significance of datasets.

3. Results

3.1. Fabrication of a 3D bioprinted hydrogel microfluidic device

To establish a realistic *in vitro* model of the gut mucosa, a perfusable hydrogel channel with villi-shaped structures was fabricated via DLP-SLA. This microfabrication technique has been previously adapted for the bioprinting of hydrogels due to its simplicity and high versatility [30–32]. The designed hydrogel reproduced a cross section of the intestinal epithelium, with a central channel (width: 1–3 mm, length: 7 mm) that mimicked the lumen and villi-like structures on the sides to support the formation of an epithelial barrier (figures 1(A) and (B)), while also allowing the encapsulation of stromal cells to represent the lamina propria. The printed channel was then encased within a microfluidic device, where two lateral channels (width: 2 mm, length: 7 mm) were defined to guarantee the perfusion of the required oxygen and nutrients for cell co-culture (figure 1(C)).

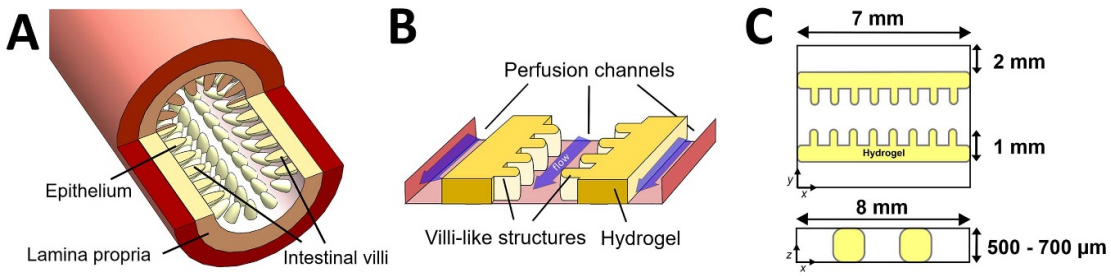

Figure 1. Biomimetic hydrogel channel for a 3D GOC model. (A) Schematic cross-section of the small intestine. (B) 3D representation of the central part of the chip with the lateral, central channels and the hydrogel. (C) Horizontal (top) and lateral (bottom) cross-sections of the central cell culture chamber.

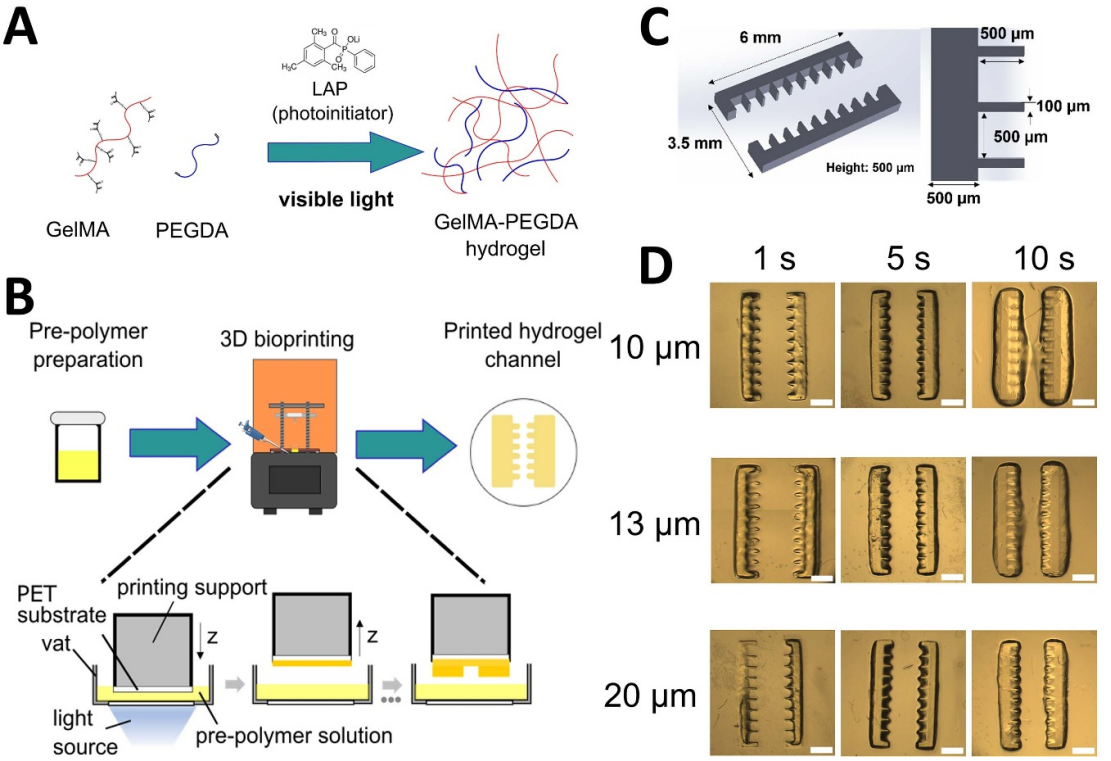

Figure 2. DLP-SLA bioprinting of hydrogel channels. (A) Schematic of the visible light-based photopolymerization reaction of PEGDA-GelMA hydrogels. (B) Illustration of the stereolithographic 3D bioprinting process to generate hydrogel channels. (C) 3D CAD model of the printed hydrogel channel. (D) Effect of layer exposure time and layer thickness on the bioprinting of hydrogel channels with lateral villi-like structures (scale bar: 1 mm).

3.1.1. Optimization of the main printing parameters for the 3D bioprinting of hydrogel channels

As a first step, the parameters to print the hydrogel channel were optimized to obtain lateral villi-like structures with high printing fidelity, using a bioink containing 5% (w/v) GelMA, 3% (w/v) PEGDA and 0.4% (w/v) LAP (figure 2(A)). To better control the photopolymerization reaction, the azo dye tartrazine was used as a photo absorber at a concentration of 0.025% (w/v). Previous work on DLP bioprinting has shown the suitability of this pre polymer solution to generate 3D hydrogel scaffolds with free-standing villi-like pillars for advanced intestinal *in vitro* models [24]. PEGDA offers long-term mechanical stability while GelMA can support cell encapsulation and attachment for cell co-culture [16, 33]. Once prepared, the bioink solution was loaded into the custom vat and the projector generated sliced light patterns of the 3D CAD design to fabricate the hydrogel in a layer-by-layer manner (figures 2(B) and S1(A)).

The layer thickness and the layer exposure time are the main printing parameters that can modulate the polymerization of the scaffolds. To assess their effect on the printed structures, a 500 μm thick hydrogel channel with lateral pillars was defined and printed (figure 2(C)). The impact of the normal layer exposure time on the fidelity of the printed lateral pillar structures was first assessed, with varying exposure times ranging from 1 s to 10 s, for a fixed layer thickness of 13 μm (figure 2(D), central row, S1(B)).

This parameter controls the energy dosage applied to the pre polymer solution from the light source, tuning the curing depth during the printing process [34]. For a layer exposure time of 1 s, the hydrogel was under polymerized and poorly defined, as the energy dose did not reach the threshold to fully cross-link the polymeric solution. The total height of the polymeric scaffold was less than 300 μm, considerably smaller than the one of the channel designs (figure S1(C)). Increasing to 5 s of exposure time significantly improved the shape of the hydrogel. The villi-like pillars approached the dimensions of the CAD design, with a length around 400 μm (figure S1(D)) and a width of around 100 μm (figure S1(E)). Lateral images of the printed hydrogels showed a total height of 540 μm approximately, with some over polymerization at the base between the pillars. However, a further increase of the layer exposure time to 10 s resulted in light overexposure, yielding polymerization of areas outside the illumination pattern, and thus significantly reducing the length of well-defined lateral pillars (figure S1(D)).

The layer thickness, also referred as the slicing thickness, was the second studied parameter to assess its effect on the printing of hydrogel channels, as it determines the total number of layers and the z resolution of the printed structures [35]. For a fixed layer exposure time of 5 s, the impact of the layer thickness on the morphology of the lateral pillars was quantified within a range between 10 μm and 20 μm (figure 2(D), central column, S1(F)). For 10 and 13 μm, it was observed that the villi-like structures had dimensions close to the ones of the CAD design, with some over polymerization at the interspace between the villi (figure S1(G), (H)). However, for thicker layers (20 μm), the hydrogel lateral shapes were slightly less defined in height, due to a reduced resolution along the z axis (figure S1(I)). Also, the hydrogels obtained with this layer thickness were much softer and prone to break apart than with shorter layer thicknesses. As a result of these printing tests, we selected 5 s of single layer exposure time and 13 μm of layer thickness as the main parameters for the optimal printing of 3D hydrogel channels, resulting in total printing times of around 6 min for 500 μm-thick hydrogel designs.

3.1.2. Assembly of the 3D hydrogel channels within a microfluidic chip

A tri channel microfluidic device was designed to place the hydrogel channel inside for dynamic cell culture (figure 3(A)). The chip was made of plastic COP using low-cost rapid prototyping techniques. After printing, the 3D hydrogel channel was encased in the central part of the chip, acting as a physical separator between the lateral channels and the central one (figure 3(B)). To ensure no leakage in between the channels, the PET substrate with the attached hydrogel was bonded to the middle piece of the chip using a double-sided PSA. Once allocated in the central chamber, a clamping system composed of two silicone sheets, two plastic COP plates and screws ensured a tight seal of the entire system (figure 3(C)).

3.1.3. Shear stress analysis in the 3D hydrogel microfluidic chip

Shear stress simulations were performed to estimate the optimal flow rate in the central channel for epithelial cell culture in the 3D GOC. To do this, a range of flow rates between 5 and 25 μl min^{-1} was set to calculate the corresponding wall shear stress on the hydrogel surfaces. Based in previous studies, a shear stress in the range of 0.01–0.025 dyn cm^{-2} was considered suitable for Caco-2 cells grown under microfluidic perfusion [36]. Two main geometries were defined for the computational study: a channel with a rectangular cross section and another one with lateral villi-like structures. For the first channel configuration, flow rates of 5–10 μl min^{-1} resulted in FSS within the optimal range, between 0.014 and 0.03 dyn cm^{-2} (figures S2(A)–(C)). In the case of the central channel with lateral villi-like structures, flow profiles were less uniform, with high flow rates in the central parts of the channel and very low ones in between the pillars (figure 3(D)), resulting in a spatial gradient of shear stress along the villus axis (figure 3(E)). Frictional forces at the tip of the villi were orders of magnitude higher than at the sides and bottom parts of the lateral structures (figure S2(D)). These observed spatial differences in FSS values are in accordance with previous 3D simulations based on biomimetic intestinal scaffolds on-chip, where the bottom regions of the villi and crypts are shielded from mechanical forces while the lateral walls and tip of the villi are exposed to the mechanical forces of peristaltic flow [37]. Based on these computed values, we selected a flow rate of 10 μl min^{-1} (for 500 μm thick hydrogels) as suitable for epithelial cell culture within the hydrogel GOC device, as higher ones could have a negative impact on the epithelial cells located at the pillar tips.

3.2. 3D bioprinted GelMA-PEGDA hydrogel channels sustain stromal cell culture under dynamic conditions

NIH-3T3 fibroblasts were selected to represent the stromal compartment of our GOC model, as they have been extensively used in co-cultures with human cells as feeder layers [38] and have been reported to enhance Caco-2 cells proliferation and differentiation via paracrine effects [16, 39]. The cells were first added to the PEGDA-GelMA pre polymer solution with a density of 7.5 $\times$ 10^6 cells ml^{-1}. A hydrogel channel with rectangular cross sections was then printed with the optimal printing parameters previously described. After the printing, the hydrogel was encased in the central chamber of the microfluidic chip for continuous cell medium perfusion with a

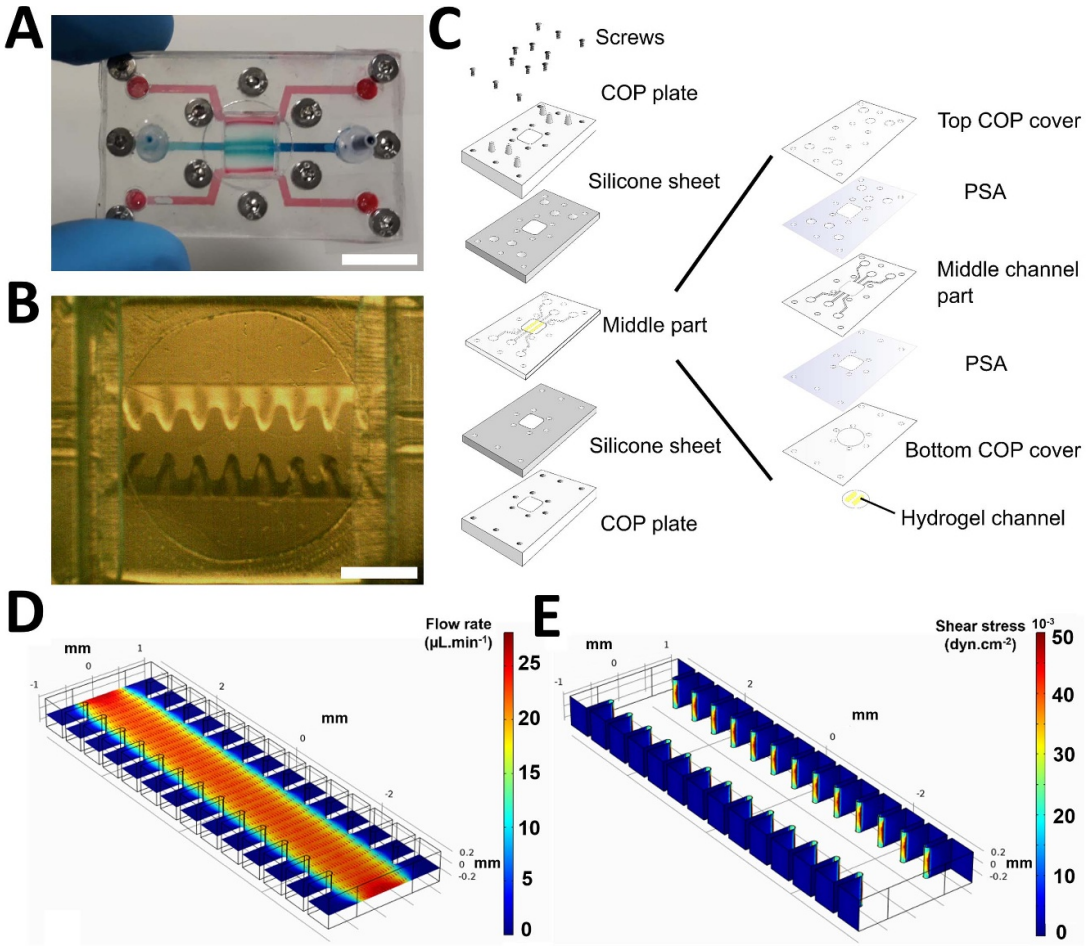

Figure 3. Assembly of the hydrogel microfluidic device. (A) Top-view photograph of the tri-channel microfluidic chip with the encapsulated hydrogel channel and perfused with different types of color dyes (scale bar: 10 mm). (B) Image of the hydrogel channel with lateral walls reproducing the shape of the intestinal villi found *in vivo* (scale bar: 2 mm). (C) Exploded view of the different components of the microfluidic chip (D) 3D view of the flow rate within the central channel. Flow rate of the channel was set to 15 μl min^{-1} and the channel width, to 2 mm. Red arrows represent the flow velocity vectors in the *XY* plane. (E) 3D representation of shear stress on the lateral walls of the hydrogel.

fluid flow of 5 μl min^{-1} along the three independent channels (figure 4(A)).

Cell viability of the 3T3 fibroblasts was assessed with a Live/Dead^{TM} assay 1 and 4 d after cell embedding (figures 4(B) and (C)). After 24 h under cell medium perfusion, most of the 3T3 cells were homogenously distributed and still alive, with cell viability rates close to 80% (figure 4(D)). Also, some cells started to spread on the surface and edges of the hydrogel channel (figure 4(B), top), in accordance with previous observations in static conditions [16, 24]. After 4 d in dynamic cell culture, a slight decrease of viable cells compared to day 1 was observed but the cell viability rate remained very high, reaching 70% (figure 4(D)). In addition, 3T3 fibroblasts migrated towards the surfaces of the hydrogel lateral walls and most of them were spread (figure 4(C)). This migration could be explained by mass transport dynamics across the hydrogel walls, generating spatial gradients of oxygen and medium concentration that induced cell movement towards the edges. Overall, these results showed that the 3D bioprinted hydrogel channels can support the cell culture of embedded fibroblasts under flow in the microfluidic device, proving their suitability for 3D GOC models.

3.3. 3D bioprinted cell-laden hydrogel channels reproduce the stromal and epithelial compartments of the intestinal mucosa in a GOC model

After assessing the cell viability of stromal cells in the hydrogel channel under dynamic conditions, we combined the encapsulation of 3T3 fibroblasts with the co-culture of Caco-2 cells on the hydrogel to recapitulate the compartmentalized structure of the intestinal mucosa in our 3D GOC model.

The printed fibroblast-laden hydrogel channel was allocated in the chip and the embedded cells were cultured under flow (5 μl min^{-1}) for 3–4 d. During this time, the 3T3 cells migrated towards the hydrogel lateral walls to better support the growth of the epithelial cells by secreting ECM proteins. Following this, the device was disconnected from the microfluidic setup and Caco-2 cells were seeded on

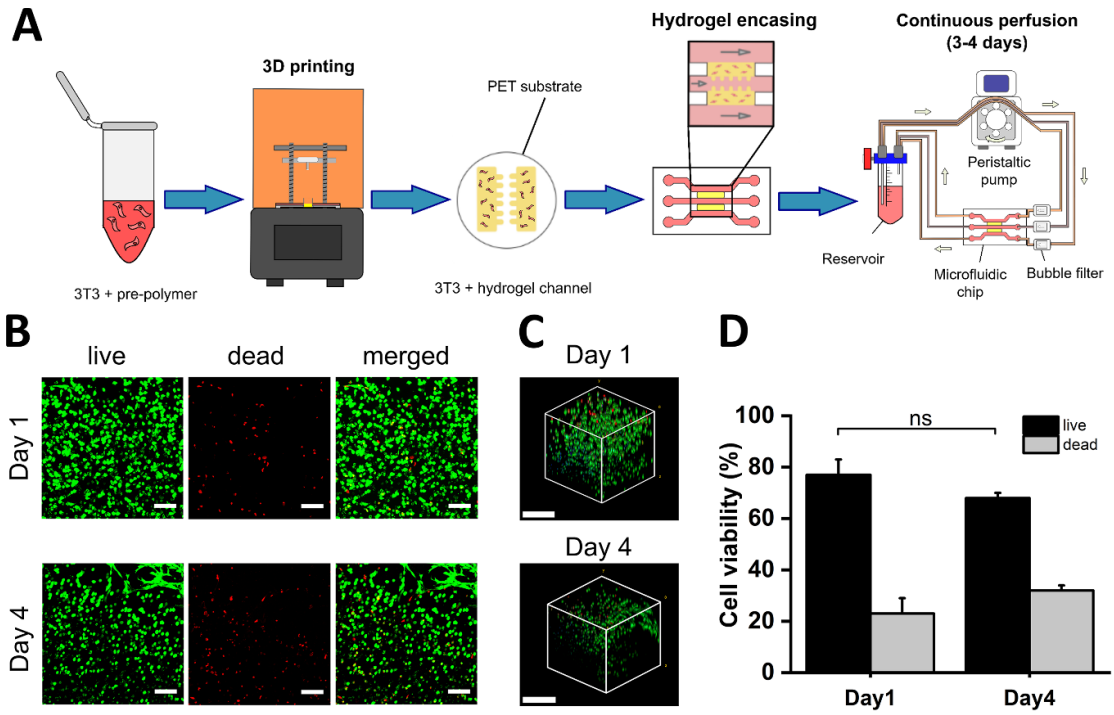

Figure 4. Cell viability of stromal cells in the hydrogel microfluidic chip. (A) Schematic illustration of the bioprinting of 3T3 cell-laden hydrogel channels and their encasement in the chip for dynamic cell culture. (B) Maximum intensity projections of encapsulated 3T3 fibroblasts at day 1 and 4 after cell culture on-chip from live/dead assays (scale bar: 100 μm). (C) 3D volume reconstruction of the 3T3 cell-laden hydrogels shown in (B). Displayed top regions of the cell-laden hydrogel interfaced with the central channel (scale bar: 250 μm). (D) Quantification of cell viability after days 1 and 4 under flow based on Live/Dead^{TM} assays. Values are the mean percentage of cell viability $\pm$ SD ($n = 3$).

the central channel with a density of 10^7 cells ml^{-1} (7.5×10^5 cells cm^{-2}). Once seeding was completed, epithelial cells were cultured under continuous perfusion for 14 d (figure 5(A)). The flow rate of lateral channels was kept to 5 μl min^{-1} to support the cell culture of hydrogel-embedded 3T3 cells while the flow in the central channel was set to 10 μl min^{-1} to obtain optimal shear stress values for epithelial cell growth inside the chip (0.01–0.025 dyn cm^{-2}). In figure 5(B), top brightfield images of the cell-laden hydrogel channel showed Caco-2 cells growing on the villi-shaped walls with the encapsulated 3T3 fibroblasts under perfusion at different days. On day 1 after epithelial cell seeding, most of the epithelial cells remained clustered in between the villi structures (figure 5(B), top). From day 5, Caco-2 cells started to partially cover the hydrogel walls, and after 12 d of cell co-culture in the chip, the epithelial cells fully covered the surface of the hydrogel walls along the central channel (figure 5(B), middle and bottom). Remarkably, epithelial cells could not form uniform barriers in the regions where the 3T3 fibroblasts were not present on the edges of the hydrogel walls (figure S3(A)), highlighting the importance of the stromal-epithelial crosstalk for the barrier formation.

To characterize the intestinal epithelial barrier covering the 3D cell-laden hydrogel channel, immunostainings were performed inside the chip after 14 d of dynamic cell culture. Fluorescence and confocal imaging of the hydrogel channel revealed the expression of tight junction and adherens junction markers ZO-1 (figure 5(C)) and β-catenin (figures 5(D) and S3(B)) lining the lateral villi-shaped walls and in certain areas of the bottom substrate, indicating the presence of an epithelial barrier. A 3D volume reconstruction of the imaged sample confirmed the presence of these cell–cell junction markers along the vertical wall of the hydrogel channel (figure 5(E)). Also, it was observed that collagen IV, a functional marker of the fibroblasts, was expressed by the 3T3 cells and found in surrounding areas close to the channel, suggesting stromal cells were capable to secrete the proteins, thus contributing to ECM remodeling and improving epithelial cell attachment (figure S3(C)). From these results, we proved the ability of our hydrogel 3D GOC system to support the dynamic cell co-culture of stromal and epithelial cells within a compartmentalized structure that mimics key spatial features of the *in vivo* intestinal mucosa.

3.4. Characterization of the barrier properties in the 3D bioprinted hydrogel GOC model

3.4.1. Apparent permeability of the intestinal barrier

To assess the integrity of the epithelial cell barrier in the 3D bioprinted GOC, we first quantified the apparent permeability P_{app} of the Caco-2 cell barrier with 3T3 fibroblasts encapsulated in rectangular-shaped hydrogel channels. After 14 d of cell co-culture under

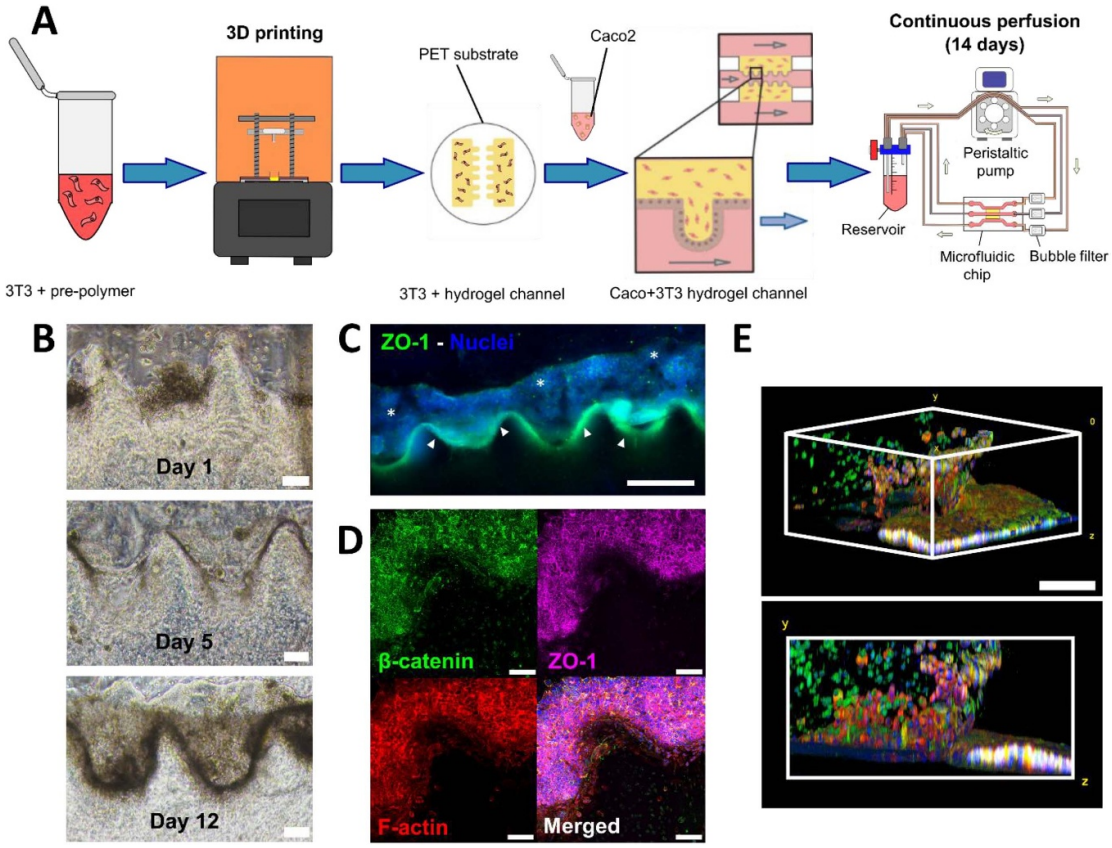

Figure 5. Epithelial barrier formation in the 3D bioprinted hydrogel GOC. (A) Schematic illustration of the co-culture process of hydrogel-embedded 3T3 fibroblasts and Caco-2 epithelial cells in the microfluidic chip. (B) Brightfield images of Caco-2 cells forming a cell barrier on the villi-shaped lateral walls of the hydrogel channel from day 1 to day 12 (scale bar: 200 μm). (C) Fluorescent top image of the Caco-2 epithelial barrier on the hydrogel channel stained for ZO-1 (green) and DAPI (blue) at day 14. (Scale bar: 500 μm). Arrow tips highlight the epithelial monolayer grown on the microstructured hydrogel walls, whereas * refer to the monolayer grown on the bottom regions. (D) Maximum intensity confocal projections of immunostainings for β-catenin (green), ZO-1 (magenta) and F-actin (red) of a co-culture on a villi-like shaped section of the hydrogel channel. DAPI (blue) was used to stain the nuclei. The image on the bottom right shows a merged display of all the markers. All samples were stained after 14 d of cell culture (scale bar: 100 μm). (E) Confocal 3D reconstructions of the immunostained sample (β-catenin in green, F-actin in red) with a perspective view (top image) and a lateral view (bottom image) (scale bar: 200 μm).

dynamic conditions, the central channel of the microfluidic chip was perfused continuously (10 μl min^{-1}) with a red fluorescent 70 kDa rhodamine-dextran solution for 90 min under a high-resolution fluorescence microscope, where images were taken at the central region of the chip to observe the radial diffusion gradient across the hydrogel (figure S4(A)). Permeability experiments with hydrogels without cells were also performed as controls.

Figure 6(A) shows the normalized fluorescence intensity profiles across the central perfusion channel and the hydrogel at different time points for both the control and the 3D multicellular intestinal model. In the regions of the hydrogel closer to the central channel, a significant increase of fluorescence intensity can be observed for the cell-free control while this increase appears slower and more moderate for the GOC. From these plots, apparent permeability values were extracted by computing the average fluorescence values in the regions of interests (figures S4(B) and (C)), showing a lower permeability for the Caco-2 epithelial barriers formed on the 3T3 cell-laden hydrogels compared to the control samples (figure 6(B)). These lower P_{app} values are associated to a higher restriction of the paracellular transport of fluorescent markers through the tight junctions, in accordance with previous studies of *in vitro* intestinal permeability on PEGDA-GelMA hydrogel constructs [16]. Overall, these results suggest the presence of a tight epithelial barrier formed on the fibroblast-laden hydrogel channel within the 3D GOC model.

3.4.2. Barrier integrity monitoring

TEER measurements were performed in real time to quantify the integrity and tightness of the intestinal epithelial barrier being formed in our 3D GOC model. Thus, we developed a new version of the previously described microfluidic chip with integrated electrodes to monitor the formation of the barrier via EIS (figure 7(A)).

A design with two coplanar electrodes placed at the lateral channels was evaluated for TEER measurements. In conventional configurations for

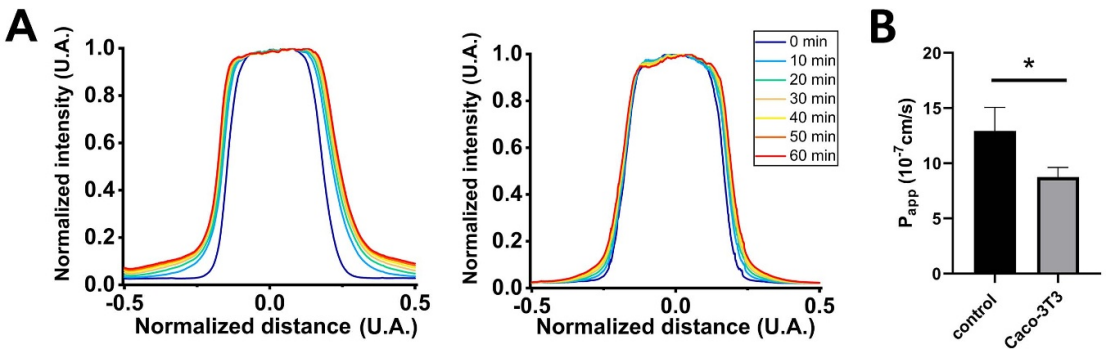

Figure 6. Apparent permeability of the epithelial barrier in the 3D hydrogel GOC. (A) Normalized fluorescence intensity profiles across the central channel without cells (left) and without a Caco-2 cell barrier in co-culture with hydrogel-embedded 3T3 fibroblasts (right). The displayed graphs represent different time points up to 1 h. (B) Apparent permeability (P_{app}) of FD70 through the epithelial barrier grown on hydrogel channels with embedded 3T3 fibroblasts under flow (Caco-3T3) and through hydrogel channels without cells (control). Values are mean ± SD ($n = 3$) * $p < 0.05$.

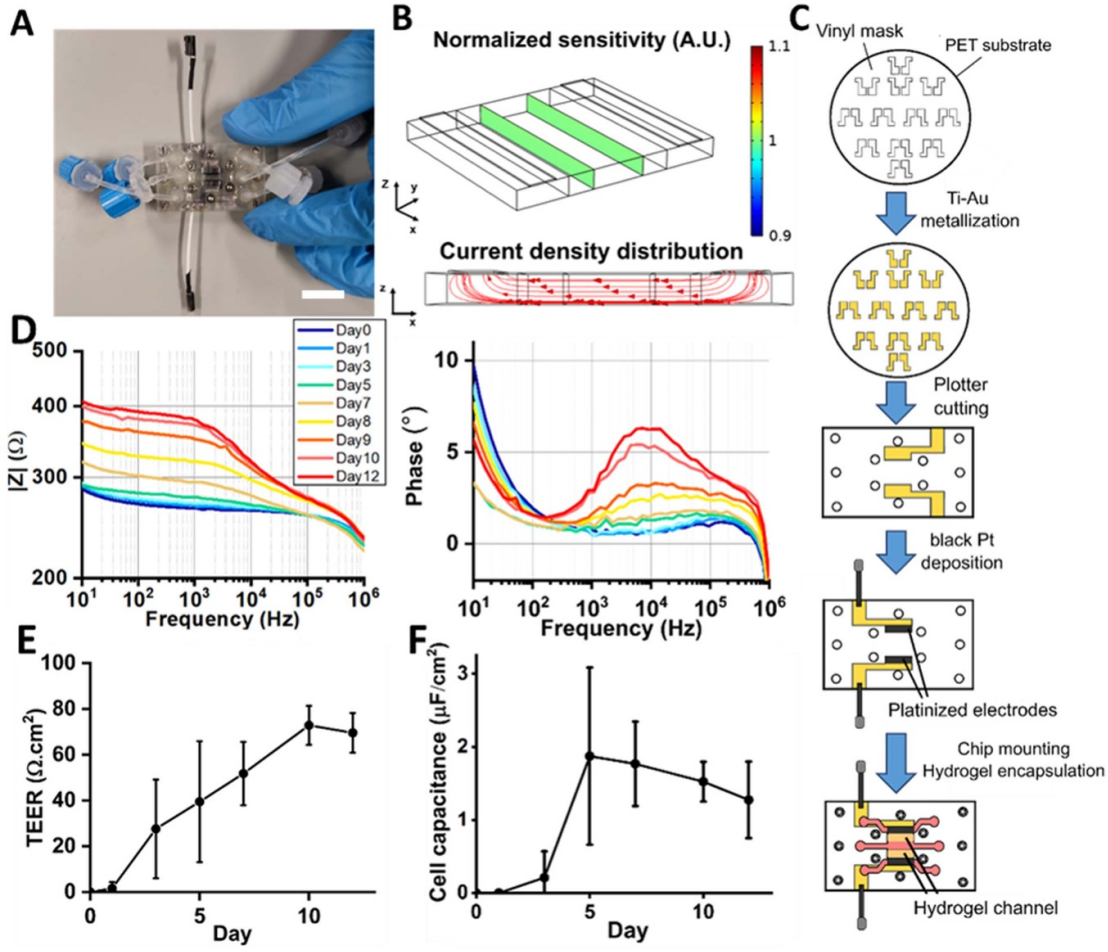

Figure 7. EIS-based TEER monitoring in the 3D hydrogel GOC. (A) Photograph of the electrode-integrated chip (scale bar: 10 mm). (B) 3D surface plot of the electrical sensitivity of the cell barrier (top) and 2D current density distribution across the hydrogel channel (bottom) for a TEER value of 10^1 Ω·cm^2. Color-displayed sensitivity values are normalized by the cell area. (C) Schematic of the fabrication and integration of the platinized gold electrodes in the chip. (D) Impedance (top) and phase (bottom) bode plots of the Caco-2 epithelial cell barrier formation with hydrogel-embedded 3T3 fibroblasts over 12 d of cell culture under flow. (E) Transepithelial electrical resistance (TEER) and (F) cell capacitance as function of cell culture time of the epithelial cell barrier. Values are normalized by the cell area and displayed as mean ± SD ($n = 3$).

organ-on-chips, integrated electrodes are generally placed at the top and bottom of the cell culture chamber, fully or partially hindering optical inspection of the cells during the experiment. As an alternative, placing the electrodes on the same substrate, but outside of the cell culture area, facilitates the fabrication

process while also allowing real time optical imaging of the whole cell culture inside the chip [40]. Since this electrode disposition has not been previously used in 3D hydrogel organ-on-chips, we performed a preliminary validation step with a FEM electrical simulation study to assess the uniformity of the current density over the cell barrier area and to identify potential TEER measurement errors (figure S5(A)). Considering a two-point measurement system, the current density distribution was computed between the electrodes for different TEER values of the cell barrier ranging from 10° to 10^3 $\Omega{\cdot}cm^2$. The electrical sensitivity was then calculated to quantify higher or lower contributions to the total TEER on the different regions of the barrier. For hydrogel heights comprised between 250 and 750 μm, the computational results showed that the normalized sensitivity was uniform and equal to 1 over the full cell barrier area for all TEER values (figures 7(B), S5(B) and (C)) while for larger heights (>2 mm), non-uniform current distributions were observed, with larger electrical sensitivities in the areas closer to the coplanar electrodes than the ones at the bottom (figure S5(D)). But these large heights were outside the usual range of hydrogel bioprinting sizes, thus not having a negative impact for the considered design in our applications. With these electrical simulations, we numerically validated the two-electrode configuration to obtain a uniform current density over the entire cell barrier area and to quantify accurately the TEER of the epithelial cell barrier.

After assessing the electrical sensitivity of the selected configuration, the electrodes were integrated in the chip via thin film deposition. Using an adhesive vinyl shadow mask, Ti–Au electrodes were patterned and fabricated on plastic substrates using e-beam evaporation. An electrochemical deposition of Pt black on the gold surface was performed to reduce the double layer capacitance of the material (figure 7(C)). By coating the electrodes with Pt black, the polarization impedance of the gold surfaces was highly reduced, allowing TEER quantification in the frequency range of interest (10^2–10^5 Hz) without the double layer effect of the electrodes (figure S6(A)). Moreover, the proper functioning of the electrodes was evaluated by measuring different PBS solutions with different molarities and testing the linear response to different electrolyte resistivities. The cell constant of the electrodes was determined by plotting the measured electrical resistance and conductivity of each sample and extracting the slope by linear regression analysis. The obtained K_{cell} value was 400.33 m^{-1}, close to the theoretical one (420.17 m^{-1}) (figure S6(B)), thus indicating a homogenous distribution of the current density and ensuring a uniform impedance measurement across a given cell culture area.

To monitor the integrity and tightness of the epithelial barrier, Caco-2 cells were initially seeded in the central channel of the microfluidic chip with the encased 3T3 fibroblast-laden hydrogel and cultured under continuous cell medium perfusion for two weeks (flow rate: 10 μl min^{-1}) (figure S6(C)). Cell impedance was measured periodically with the integrated platinized gold electrodes from the seeding of the epithelial cells (day 0) up to day 14 at different frequencies ranging from 10 Hz to 1 MHz.

The obtained impedance plots were then analyzed to extract the main electrical parameters of the cell barrier: the TEER and the cell layer capacitance C_{cl} [41]. To do that, an equivalent electrical circuit was used to fit the data to a theoretical model. In this model, a resistance representing TEER is placed in parallel with a constant phase element (CPE) representing the cell layer capacitance, both in series with the cell medium resistance R_s (figure S6(D)) [42]. The mathematical expression of the CPE is:

$$Z_{CPE} = \frac{1}{K(jw)^{\alpha}}$$

where K is the admittance, w is the angular frequency, j is the imaginary unit and α is an exponent corresponding to 0 or 1 for an ideal resistor or an ideal capacitance respectively. The electrical equivalent model fitting was performed in the range between 10^2 and 10^5 Hz using a least squares regression method (PSTrace software). Within these frequencies, the resistive and capacitive behavior of the cell barrier dominates over the electrode impedance and the resistance of the cell medium. After fitting, the cell layer capacitance was determined as follows:

$$C_{cl} = \frac{(K * \mathrm{TEER})^{\frac{1}{\alpha}}}{\mathrm{TEER}}$$

where K is the admittance of the CPE and α is the exponent of the CPE. Both TEER and C_{cl} were normalized by the area of the cell barrier to compare them to other values reported in the literature.

Caco-2 cells seeded on the rectangular-shaped hydrogel channels started to attach and expand on the lateral walls in close contact with the encapsulated 3T3 cells, forming an epithelial barrier from day 7 that reached confluency at day 12 (figure S6(E)). The observed barrier formation was correlated with the measured impedances inside the chip (figure 7(D)). In the initial days of cell co-culture, from day 0 to day 5, the recorded impedance magnitude was flat, as epithelial cells had not fully covered the hydrogel surface yet. From day 6 onwards, the total impedance increased in the lower frequencies (10^2–10^3 Hz), indicating that Caco-2 cells formed a tighter barrier. Also, in the middle frequencies (10^3–10^5 Hz), a significant increase of the impedance was observed, as cells covered the hydrogel surface and formed a confluent barrier. This effect was also visible in the impedance phase spectra, with a progressive phase increase in the corresponding frequencies (figure 7(D)).

Applying the selected equivalent electrical model on the impedance magnitude plots within the 10^2–10^5 Hz frequency range, TEER and cell capacitance C_{cl} values of the epithelial barrier were extracted for different days of cell culture on-chip. During the first days of cell co-culture, TEER values were low, with a slow increase up to 20 $\Omega \cdot cm^2$. From day 5–6, TEER increased faster as cells were forming a tight barrier, reaching values up to 80 $\Omega \cdot cm^2$ at day 12, similar to *in vivo* measurements of the native small intestine (figure 7(E)) [3]. This trend of cell barrier resistance increase is consistent with previous intestinal *in vitro* studies based on stromal-cell laden 3D hydrogels, where a boost in TEER was observed at day 9–11, according to the time the fibroblasts needed to migrate towards the surface of the hydrogel and to secrete ECM proteins for epithelial cell attachment [24]. Moreover, the cell capacitance also increased significantly within the first week of cell culture on-chip, as cells gradually covered the hydrogel surface (figure 7(F)). After the first 7 d, C_{cl} reached a plateau, with values close to 2 $\mu F\ cm^{-2}$. Cell capacitance in mature barriers is constant and close to 1 $\mu F\ cm^{-2}$ for flat cell monolayers. Higher values in epithelial intestinal models with Caco-2 cells have also been reported and attributed to an increased cell surface due to the formation of microvilli at the apical brush border. Hence, these results could also suggest Caco-2 cells formed a polarized tight barrier in our 3D GOC model. Overall, these results show Caco-2 cells can form a functional and mature intestinal epithelial barrier in the presence of fibroblasts within our 3D hydrogel GOC system, offering a powerful model for physiological and pathological studies of the small intestine.

4. Conclusion

Here, we presented a 3D bioprinted GOC system with a perfusable hydrogel channel containing villi-like structures that recapitulates the compartmentalized structure of the intestinal mucosa. A customized visible-light DLP-SLA printing setup was used with a photosensitive PEGDA-GelMA bioink to generate the hydrogels in a simple and reliable manner. This fabrication technique is compatible with microfluidic integration for dynamic *in vitro* studies. By using this approach, the chip could support the co-culture of hydrogel-embedded stromal cells and intestinal epithelial cells for 2 weeks under perfusion, resulting in the formation of a tight intestinal barrier.

The proposed hydrogel GOC was also adapted for real time TEER monitoring by integrating electrodes inside the device. Current GOC models with incorporated 3D hydrogels do not include such sensing capabilities, resulting in low readouts for long-term experiments. With our device, a significant and progressive increase of the cell layer impedance linked to the formation of the epithelial barrier was recorded for 2 weeks. In addition, unlike standard approaches where electrodes are placed at the top and bottom of the cell culture area, the coplanar configuration of our electrodes allowed clear optical imaging of the epithelial cells and hydrogel-encapsulated fibroblasts. The presented system is highly versatile as it can be adapted to other studies such as microbial–intestinal interactions and to other tissue barriers *in vitro* to quantitatively assess their properties in real time, with potential applications in disease modeling and drug screening studies.

Data availability statement

All data that support the findings of this study are included within the article (and any supplementary files).

Acknowledgments

Funding for this project was provided by a European Union Horizon 2020 ERC Grant (Agreement 647863—COMIET), the CERCA Programme/Generalitat de Catalunya (2017-SGR-1079), and the Spanish Ministry of Economy and Competitiveness (PID2021-129115OB-I00). The authors acknowledge support from the Ministerio de Ciencia Innovacion y Universidades, in Spain, through GUMICHIP project (RTI2018-096786-B-I00 funded by MCIN/AEI/10.13039/501100011033 and by 'ERDF A way of making Europe'). D V acknowledge that this work has been done in the framework of the PhD in Electrical and Telecommunication Engineering at the Universitat Autònoma de Barcelona. D V was supported by the Marie Skłodowska-Curie COFUND PhD fellowship (Grant Agreement 754397). N T acknowledges the Spanish Ministry of Science and Innovation, Juan de la Cierva program (Grant IJC2019-040289-I). This research was supported by CIBER -Consorcio Centro de Investigación Biomédica en Red- (CB06/01/0049), Instituto de Salud Carlos III, Ministerio de Ciencia e Innovación. The results presented here only reflect the views of the authors; the European Commission is not responsible for any use that may be made of the information it contains.

ORCID iDs

María García-Díaz https://orcid.org/0000-0002-4794-5437
Núria Torras https://orcid.org/0000-0001-5027-7428

Mar Alvarez https://orcid.org/0000-0003-4590-4401
Elena Martinez https://orcid.org/0000-0002-6585-4213

References

[1] Volk N and Lacy B 2017 Anatomy and physiology of the small bowel *Gastrointest. Endosc. Clin. North Am.* **27** 1–13
[2] Odenwald M A and Turner J R 2016 The intestinal epithelial barrier: a therapeutic target? *Nat. Rev. Gastroenterol. Hepatol.* **14** 9–21
[3] Hilgers A, Conradi R A and Burton P S 1990 Caco-2 cell monolayers as a model for drug transport across the intestinal mucosa *Pharm. Res.* **7** 902–10
[4] Hidalgo I J, Raub T J and Borchardt R T 1989 Characterization of the human colon carcinoma cell line (Caco-2) as a model system for intestinal epithelial permeability *Gastroenterology* **96** 736–49
[5] Costa J and Ahluwalia A 2019 Advances and current challenges in intestinal *in vitro* model engineering: a digest *Front. Bioeng. Biotechnol.* **7** 456869
[6] Ashammakhi N, Nasiri R, Barros N R D, Tebon P, Thakor J, Goudie M, Shamloo A, Martin M G and Khademhosseini A 2020 Gut-on-a-chip: current progress and future opportunities *Biomaterials* **255** 120196
[7] Bein A, Shin W, Jalili-Firoozinezhad S, Park M H, Sontheimer-Phelps A, Tovaglieri A, Chalkiadaki A, Kim H J and Ingber D E 2018 Microfluidic organ-on-a-chip models of human intestine *Cell. Mol. Gastroenterol. Hepatol.* **5** 659–68
[8] Peterson L W and Artis D 2014 Intestinal epithelial cells: regulators of barrier function and immune homeostasis *Nat. Rev. Immunol.* **14** 141–53
[9] Powell D W, Pinchuk I V, Saada J I, Chen X and Mifflin R C 2011 Mesenchymal cells of the intestinal lamina propria *Annu. Rev. Physiol.* **73** 213
[10] Kim H J, Li H, Collins J J and Ingber D E 2016 Contributions of microbiome and mechanical deformation to intestinal bacterial overgrowth and inflammation in a human gut-on-a-chip *Proc. Natl Acad. Sci. USA* **113** E7–15
[11] Shah P *et al* 2016 A microfluidics-based in vitro model of the gastrointestinal human-microbe interface *Nat. Commun.* **7** 11535
[12] Maurer M *et al* 2019 A three-dimensional immunocompetent intestine-on-chip model as in vitro platform for functional and microbial interaction studies *Biomaterials* **220** 119396
[13] Terrell J A, Jones C G, Kabandana G K M and Chen C 2020 From cells-on-a-chip to organs-on-a-chip: scaffolding materials for 3D cell culture in microfluidics *J. Mater. Chem.* B **8** 6667–85
[14] Caliari S R and Burdick J A 2016 A practical guide to hydrogels for cell culture *Nat. Methods* **13** 405–14
[15] Tibbitt M W and Anseth K S 2009 Hydrogels as extracellular matrix mimics for 3D cell culture *Biotechnol. Bioeng.* **103** 655–63
[16] Vila A *et al* 2020 Hydrogel co-networks of gelatine methacrylate and poly(ethylene glycol) diacrylate sustain 3D functional in vitro models of intestinal mucosa *Biofabrication* **12** 025008
[17] Vera D, García-Díaz M, Torras N, Álvarez M, Villa R and Martinez E 2021 Engineering tissue barrier models on hydrogel microfluidic platforms *ACS Appl. Mater. Interfaces* **13** 13920–33
[18] Trietsch S J *et al* 2017 Membrane-free culture and real-time barrier integrity assessment of perfused intestinal epithelium tubes *Nat. Commun.* **8** 262
[19] Shim K-Y, Lee D, Han J, Nguyen N-T, Park S and Sung J H 2017 Microfluidic gut-on-a-chip with three-dimensional villi structure *Biomed. Microdevices* **19** 37
[20] Nikolaev M *et al* 2020 Homeostatic mini-intestines through scaffold-guided organoid morphogenesis *Nature* **585** 574–8
[21] Marrero D, Pujol-Vila F, Vera D, Gabriel G, Illa X, Elizalde-Torrent A, Alvarez M and Villa R 2021 Gut-on-a-chip: mimicking and monitoring the human intestine *Biosens. Bioelectron.* **181** 113156
[22] Henry O Y F, Villenave R, Cronce M J, Leineweber W D, Benz M A and Ingber D E 2017 Organs-on-chips with integrated electrodes for trans-epithelial electrical resistance (TEER) measurements of human epithelial barrier function *Lab Chip* **17** 2264–71
[23] van der Helm M W *et al* 2019 Non-invasive sensing of transepithelial barrier function and tissue differentiation in organs-on-chips using impedance spectroscopy *Lab Chip* **19** 452–63
[24] Torras N, Zabalo J, Abril E, Carré A, García-Díaz M and Martínez E 2023 A bioprinted 3D gut model with crypt-villus structures to mimic the intestinal epithelial-stromal microenvironment *Biomater. Adv.* **153** 213534
[25] Loessner D, Meinert C, Kaemmerer E, Martine L C, Yue K, Levett P A, Klein T J, Melchels F P W, Khademhosseini A and Hutmacher D W 2016 Functionalization, preparation and use of cell-laden gelatin methacryloyl-based hydrogels as modular tissue culture platforms *Nat. Protocols* **11** 727–46
[26] Yeste J, Martínez-Gimeno L, Illa X, Laborda P, Guimerà A, Sánchez-Marín J P, Villa R and Giménez I 2018 A perfusion chamber for monitoring transepithelial NaCl transport in an in vitro model of the renal tubule *Biotechnol. Bioeng.* **115** 1604–13
[27] Yeste J, Illa X, Gutiérrez C, Solé M, Guimerà A and Villa R 2016 Geometric correction factor for transepithelial electrical resistance measurements in transwell and microfluidic cell cultures *J. Phys. D: Appl. Phys.* **49** 375401
[28] Gabriel G, Erill I, Caro J, Gómez R, Riera D, Villa R and Godignon P 2007 Manufacturing and full characterization of silicon carbide-based multi-sensor micro-probes for biomedical applications *Microelectron. J.* **38** 406–15
[29] Nicolas A *et al* 2021 High throughput transepithelial electrical resistance (TEER) measurements on perfused membrane-free epithelia *Lab Chip* **21** 1676–85
[30] Soman P, Chung P H, Zhang A P and Chen S 2013 Digital microfabrication of user-defined 3D microstructures in cell-laden hydrogels *Biotechnol. Bioeng.* **110** 3038–49
[31] Bhusal A, Dogan E, Nguyen H-A, Labutina O, Nieto D, Khademhosseini A and Miri A K 2021 Multi-material digital light processing bioprinting of hydrogel-based microfluidic chips *Biofabrication* **14** 014103
[32] Grigoryan B *et al* 2019 Multivascular networks and functional intravascular topologies within biocompatible hydrogels *Science* **364** 458–64
[33] Wang Z, Abdulla R, Parker B, Samanipour R, Ghosh S and Kim K 2015 A simple and high-resolution stereolithography-based 3D bioprinting system using visible light crosslinkable bioinks *Biofabrication* **7** 045009
[34] Ng W L, Lee J M, Zhou M, Chen Y-W, Lee K-X A, Yeong W Y and Shen Y-F 2020 Vat polymerization-based bioprinting—process, materials, applications and regulatory challenges *Biofabrication* **12** 022001
[35] Gong H, Bickham B P, Woolley A T and Nordin G P 2017 Custom 3D printer and resin for 18 μm $\times$ 20 μm microfluidic flow channels *Lab Chip* **17** 2899–909
[36] Delon L C, Guo Z, Oszmiana A, Chien C-C, Gibson R, Prestidge C and Thierry B 2019 A systematic investigation of the effect of the fluid shear stress on Caco-2 cells towards the optimization of epithelial organ-on-chip models *Biomaterials* **225** 119521
[37] Costello C M, Phillipsen M B, Hartmanis L M, Kwasnica M A, Chen V, Hackam D, Chang M W, Bentley W E and March J C 2017 Microscale bioreactors for in situ characterization of GI epithelial cell physiology *Sci. Rep.* **7** 1–10

[38] Hynds R E, Bonfanti P and Janes S M 2018 Regenerating human epithelia with cultured stem cells: feeder cells, organoids and beyond *EMBO Mol. Med.* **10** 139–50
[39] Göke M, Kanai M and Podolsky D K 1998 Intestinal fibroblasts regulate intestinal epithelial cell proliferation via hepatocyte growth factor *Am. J. Physiol.* **274** G809–18
[40] Yeste J, García-Ramírez M, Illa X, Guimerà A, Hernández C, Simó R and Villa R 2018 A compartmentalized microfluidic chip with crisscross microgrooves and electrophysiological electrodes for modeling the blood-retinal barrier *Lab Chip* **18** 95–105
[41] Grimnes S and Martinsen Ø G 2014 Bioimpedance and bioelectricity basics *Bioimpedance and Bioelectricity Basics* 3rd edn (Academic) pp 1–563
[42] Gerasimenko T, Nikulin S, Zakharova G, Poloznikov A, Petrov V, Baranova A and Tonevitsky A 2020 Impedance spectroscopy as a tool for monitoring performance in 3D models of epithelial tissues *Front. Bioeng. Biotechnol.* **7** 474